01 Jun 2023

Automated Detection and Characterization of Cracks on Concrete using Laser Scanning

Yunfeng Ge

Jenny Liu
Missouri University of Science and Technology, jennyliu@mst.edu

Xiong Zhang
Missouri University of Science and Technology, zhangxi@mst.edu

Huiming Tang

et. al. For a complete list of authors, see https://scholarsmine.mst.edu/civarc_enveng_facwork/2264

Recommended Citation

Y. Ge et al., "Automated Detection and Characterization of Cracks on Concrete using Laser Scanning," *Journal of Infrastructure Systems*, vol. 29, no. 2, article no. 4023005, American Society of Civil Engineers, Jun 2023.
The definitive version is available at https://doi.org/10.1061/JITSE4.ISENG-1936

ASCE

Automated Detection and Characterization of Cracks on Concrete Using Laser Scanning

Yunfeng Ge[1]; Jenny Liu, M.ASCE[2]; Xiong Zhang, M.ASCE[3]; Huiming Tang[4]; and Xiaolong Xia[5]

Abstract: Accurate crack detection and characterization on concrete are essential for the maintenance, safety, and serviceability of various infrastructures. In this paper, an innovative approach was developed to automatically measure the cracks from 3D point clouds collected by a phase-shift terrestrial laser scanner (TLS) (FARO Focus3D S120). The approach integrates several techniques to characterize the cracks, which include the deviation on point normal determined using k-nearest neighbor (kNN) and principal components analysis (PCA) algorithms to identify the cracks, and principal axes and curve skeletons of cracks to determine the projected and real dimensions of cracks, respectively. The coordinate transformation was then performed to estimate the projected dimensions of cracks. Curve skeletons and cross sections of cracks were extracted to represent the real dimensions. Two cases of surface cracks were used to validate the developed approach. Because of the differences in definitions of the crack dimension in the three methods and due to the curve shape of the crack, the width and depth of cracks obtained from the cross-section method and manual measurement were close but slightly smaller than those measured by the projection algorithm; whereas the length of cracks determined by the curve-skeletons method was slightly larger than those obtained by the manual measurement and projection method. The real dimension of a crack has good agreements with real situations when compared with the results of the manual measurement and projection method. **DOI: 10.1061/JITSE4.ISENG-1936.**

Author keywords: Cracks; Automated detection; Automated characterization; Laser scanning; Point clouds; Point normal variance.

Introduction

Cracking by far makes up the majority of failure issues in many infrastructures such as pavements, bridges, structures, and tunnels because of its tendency to spread and the wide variety of elements that can cause cracking. Accurately detecting, continually monitoring, and timely assessing cracking before the *critical condition* is reached, extends the service life of infrastructure and reduces lifecycle costs, gives transportation authorities the information they need to maintain it more effectively and economically, allows engineers to intervene before a catastrophic failure, and provides a better understanding of the performance of assets to inform future designs and materials.

To date, the detection of crack dimensions and patterns can be classified into two major categories: contact and noncontact methods. In the contact methods, traditionally transportation infrastructures are visually inspected and manually maintained under traffic control with the aid of heavy lifting equipment or costly inspection equipment. Some contact inspection methods, such as crack magnifiers (Valença et al. 2013), width rulers (Nakaniwa et al. 2014), feeler gauges (Bandis et al. 1983), and electronic sensors (Ritdumrongkul and Fujino 2007), can provide enough precision for crack measurement with low costs and easy operation. However, these techniques suffer from several challenges, such as: (1) The measurement range is limited; thus, they are not suitable for large-scale crack measurement, (2) Direct contact is required during the measuring process, and it is difficult and dangerous to map the cracks in inaccessible regions, and (3) It is always laborious and time-consuming (Yang et al. 2018). For instance, it is not uncommon to take several days to measure the width of cracks on a bridge cap, due to numerous preparatory work (e.g., traffic restriction and safety protection), and large quantity of measurements needed along a long crack. With the advances in electrooptical technology in the past few decades, diverse noncontact methods are available to determine the location and geometries of cracks, including two-dimensional (2D) image processing techniques and analysis of reconstructed three-dimensional (3D) data (Nishiyama et al. 2015; Napolitano and Glisic 2019). 2D image analysis is very popular for crack detection due to its versatility and extremely low cost. Based on the assumptions that the crack has a lower intensity than the local background and the crack represents a sharp change in intensity, various numerical algorithms and detection methods have been developed. Some examples include intensity thresholding methods (Oliveira and Correia 2009), segmentation-based approaches (Kirschke and Velinsky 1992), filter-based algorithms (Zalama et al. 2014), minimal-path methods (Avila et al. 2014),

[1]Associate Professor, Faculty of Engineering, China Univ. of Geosciences, Wuhan, Hubei 430074, China; Visiting Scholar, Dept. of Civil, Architectural, and Environmental Engineering, Missouri Univ. of Science and Technology, Rolla, MO 65409. ORCID: https://orcid.org/0000-0003-4390-6841. Email: geyunfeng@cug.edu.cn; ygbkp@mst.edu

[2]Professor, Dept. of Civil, Architectural, and Environmental Engineering, Missouri Univ. of Science and Technology, Rolla, MO 65409. ORCID: https://orcid.org/0000-0002-3840-1438. Email: jennyliu@mst.edu

[3]Professor, Dept. of Civil, Architectural, and Environmental Engineering, Missouri Univ. of Science and Technology, Rolla, MO 65409 (corresponding author). Email: zhangxi@mst.edu

[4]Professor, Faculty of Engineering, China Univ. of Geosciences, Wuhan, Hubei 430074, China. Email: tanghm@cug.edu.cn

[5]Ph.D. Candidate, Dept. of Civil, Architectural, and Environmental Engineering, Missouri Univ. of Science and Technology, Rolla, MO 65409. Email: xxrkq@mst.edu

Note. This manuscript was submitted on December 27, 2020; approved on October 26, 2022; published online on January 24, 2023. Discussion period open until June 24, 2023; separate discussions must be submitted for individual papers. This paper is part of the ***Journal of Infrastructure Systems***, © ASCE, ISSN 1076-0342.

texture-anisotropy approach (Nguyen et al. 2009), the CrackTree (Zou et al. 2012), artificial neural network (Kaseko and Ritchie 1993; Lee and Lee 2004; Dung 2019), support vector machine (Li et al. 2017; Hoang et al. 2018), and deep learning (Zhang et al. 2016; Huang et al. 2018; Cha et al. 2017). However, all these image-based methods only consider the color data overlooking the importance of geometric information, which leads to a gap when applying them to existing structures (Valença et al. 2017). Nevertheless, all infrastructures and cracks on them are three-dimensional (3D). 2D image analyses cannot provide accurate 3D measurements for advanced analyses (Valença et al. 2017; Mohan and Poobal 2018).

The limitations of 2D image processing techniques bring out the advent of 3D reconstruction, which are less vulnerable to lighting conditions and present more useful information and fewer noises in terms of crack detection (Wang 2004; Zhang et al. 2019). The depth-checking methods (Jahanshahi et al. 2013), interactive crack detection algorithm (Zhang et al. 2017b), hybrid crack detection procedures (Sollazzo et al. 2016), and 3D shadow modeling (Zhang et al. 2017a) were all proposed in recent years for detecting cracks on 3D surfaces. However, it is difficult to use these algorithms to detect cracks on multiple surfaces. The cracks with low elevation on a horizontal surface were accurately identified based on the depth information. However, it was difficult to detect the cracks on a vertical wall using the depth data (Zhang et al. 2017a).

The 3D reconstruction of cracks can be performed using photogrammetry which is a technique to build the 3D model of physical objects from 2D image sequences. However, like the 2D image methods, the resolution and precision of the 3D model of cracks are easily affected by the ambient environment, image quality, and photographic camera. To capture details of the crack morphology, a large quantity of images within a short distance (Jiang et al. 2008) are needed, and the analyses are computationally intensive. Another technique of 3D reconstruction, laser scanning, a remote sensing technique, can make a long-distance measurement with high resolution. Recently, it has gained more attention in civil and geological engineering areas as a promising tool to reconstruct the 3D model of cracks by collecting the dense point clouds of concrete surfaces (Laefer et al. 2014; Gui et al. 2018; Ge et al. 2018). Olsen et al. (2010) mapped the cracks on concrete based on the intensity of the point cloud which provided a sharp contrast between unruptured surfaces and cracks. Kim et al. (2014) employed both angle and distance deviations to locate the regular defects (square and round shapes) on concrete surfaces under experimental conditions. Jovančević et al. (2017) detected the dents and scratches from point clouds using a region growing algorithm in which the local normal and curvature parameters were used as the evaluation indexes. Artificial intelligence algorithms have also been introduced to analyze the point clouds for cracks recognition, such as the wavelet neural network (Laflamme et al. 2012), recurrent neural network (Zhang et al. 2019), and deep learning (Zhang et al. 2017b; Fei et al. 2019).

Although laser scanning has demonstrated its effectiveness in cracks detection in previous studies, some methods were performed in the laboratory environment, which had difficulties in identifying complete cracks over the whole region (Zou et al. 2012). In addition, 3D reconstruction always involves a huge number of points, and some undesired noises are also introduced during data collection, resulting in the inefficiency and limitations of data processing (Rabah et al. 2013). More research efforts are needed to refine and improve for the purpose of practical application.

Properly characterizing cracks to find the 3D dimensions of cracks is critical as well. Cracks are often curving rather than straight lines, and their 3D geometry changes irregularly. It is therefore inaccurate to measure the crack using the projected dimensions. At present, most studies focused on crack detection. However, the characterization of cracks after they are detected has been rarely further investigated due to the complexity and diversity of crack patterns. In addition, 2D image analyses discussed previously cannot provide accurate 3D models for cracks and therefore cannot be used for accurate crack characterization.

Hence, the objective of this study was to develop an innovative approach to automatically map the cracks on concrete structures based on the 3D point clouds gathered using laser scanning, and accurately characterize cracks including their projected and real dimensions. In this paper, a surface crack was used as an example to navigate the procedures of image data collection, processing, and analysis. A conventional crack survey was then conducted to validate the results obtained from this approach. The paper further presents a case study of detecting and characterizing more complicated cracks to demonstrate the feasibility of this approach.

Methodology and Procedures

In this study, a method was developed to automatically identify and measure the cracks on concrete structures from point clouds collected by laser scanning. Two main steps are involved in this method: crack detection and crack characterization (Fig. 1). In the first step of crack detection, the point clouds of cracks and concrete structures are collected using a terrestrial laser scanner (TLS). The normal vector of each point is calculated using the k-nearest neighbor (kNN) and principal components analysis (PCA) algorithms. All objects with a significant change of point normal are then extracted from the point clouds based on the normal variance, including cracks, dents, and horizontal edges (intersections of different planes). The small-scale dents can be removed by setting a volume threshold. As for the horizontal edges which do not belong to cracks, they can be removed by specifying a specific location range because these edges have regular shapes and similar z-axis values. In the second step of crack characterization, a coordinate

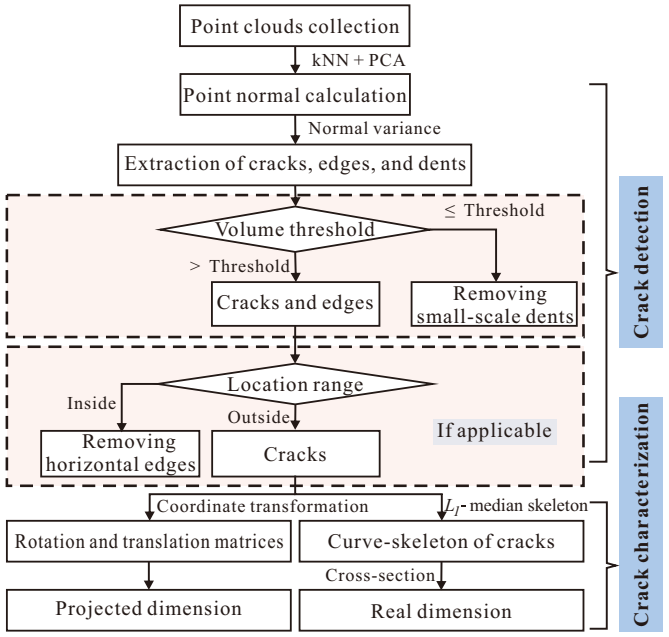

Fig. 1. Flow chart of the proposed method in this study.

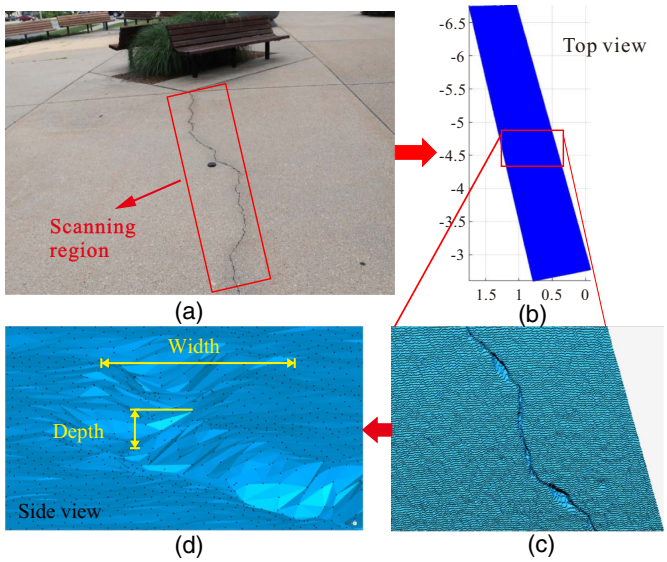

Fig. 2. Point cloud collection of cracks on a concrete ground: (a) scanning region; (b) top view of point cloud in the scanning region; (c) details of point cloud in the crack region; and (d) side view of point cloud in the scanning region.

transformation algorithm is used to determine the rotation and translation matrices, and the projected dimension of cracks is then measured to roughly estimate the area of cracks. In addition, L_1-median skeleton algorithms are used to find the curve-skeleton of cracks to calculate the actual length of cracks, and 10 cross sections are randomly selected to determine the actual width and depth. An example was next used to elaborate the procedures.

Point Clouds Collection

A surface crack located on a paved concrete ground in a building entrance area was selected to demonstrate the procedures of the developed approach. This crack was in a curved shape with an average length of 4.180 m and an average width of 0.009 m. Fig. 2(a) shows the crack, and the area within a red rectangle is the scanning region. A phase-shift TLS (FARO Focus3D S120) was used to collect the point cloud of this crack. The maximum measuring range of this scanner is 120 m under the conditions of low ambient light and normal incidence. Its resolution-the interval between adjacent points, can reach 0.3 mm at a 10 m scanning distance. Scanning parameters and basic information of the raw point cloud are listed in Table 1. Fig. 2(b) shows the top view of the point cloud of the scanning region on the ground collected using this scanner. Total of 527,320 effective points were generated for this area after denoising, allowing capture of the details of geometry information for this crack [Fig. 2(c)]. Fig. 2(d) shows the point cloud of the same scanning region from the side view. As depicted in Figs. 2(c and d), the crack can be distinguished from point clouds based on the difference in geometric irregularity and discontinuity between the crack and the surroundings. The laser can even reach the inside of cracks to collect point clouds, which is usually difficult for normal image-based techniques due to the low illumination.

Point Normal Calculation

Several parameters are available to describe the discontinuous geometry of cracks, including point normal, point curvature, point intensity, and depth. Fig. 3 compares the sensitivity of these parameters with this example crack. As shown in Fig. 3, the magnitude of point normal on the crack was larger than that on the surrounding surface, and the direction of point normal was different between the crack area and noncrack area, indicating the point normal has adequate robustness to capture the difference between the cracks and the surroundings. Nevertheless, the crack and noncrack areas were difficult to distinguish using the other three parameters (i.e., point curvature, point intensity, and point depth). Thus, the point normal was selected for the purpose of crack detection in this study.

The normal of a point is represented by the normal of the fitting plane to this point and its neighbors. For the grid data (organized point clouds), four-connected or eight-connected points can be treated as neighbors. In addition, the surrounding points can be determined using the kNN algorithm by specifying the number of closest points or searching radius in the origin point clouds. In this study, to avoid the interpolation errors caused by data griding, the kNN algorithm was used to search the N, the number of nearest neighbor points of a query point. The kNN algorithm is a nonparameter classification approach and has been widely used in many applications (Deng et al. 2016). It has been programmed into MATLAB as a function called knnsearch. The normal of the query point was then determined by calculating the normal of the fitting plane to the point set (query point and its neighbor points). Estimation of point normal was therefore reduced to an implementation of the PCA of the point set, and the eigenvector corresponding to the smallest eigenvalue of the covariance matrix of the point set was the point normal (Klasing et al. 2009). PCA algorithm relates the process of determining the principal components of the given data and can be performed by the pca function in MATLAB. Geometrically, the points on the concrete plane featured a similar normal direction which was approximately perpendicular to the plane and a similar normal magnitude as shown in Fig. 3(a). Thus, the places with significant changes in normal (high normal deviation) are regarded as the crack area. The direction and magnitude of the point normal in this area are different from those in the concrete plane due to the geometric irregularity and discontinuity.

Cracks and Dents Extraction Based on Point Normal Variance

Significant changes of point normal occur on the cracks and dents (small-scale damaged areas) due to the geometrical discontinuity, whereas the points on the concrete plane have similar normal values. Therefore, the point normal variance can be used as an indicator to describe the changes in these features. For a given point, the point normal variance $[Var(n_p)]$ can be calculated by Eq. (1):

Table 1. Summary of scan parameters and point clouds for two cases

Cases	Resolution setting	Quality	Speed (kpt/s)	Scan time	Scan size (pt)	Resolution (mm/10 m)	File size (MB)	Point amount
Ground surfaces	1/2	4×	122	5 min and 46 s	1,702 × 4,127	3.068	345	5,858,350
Stair	1/2	3×	244	2 min and 11 s	848 × 1,994	3.068	89	1,585,865

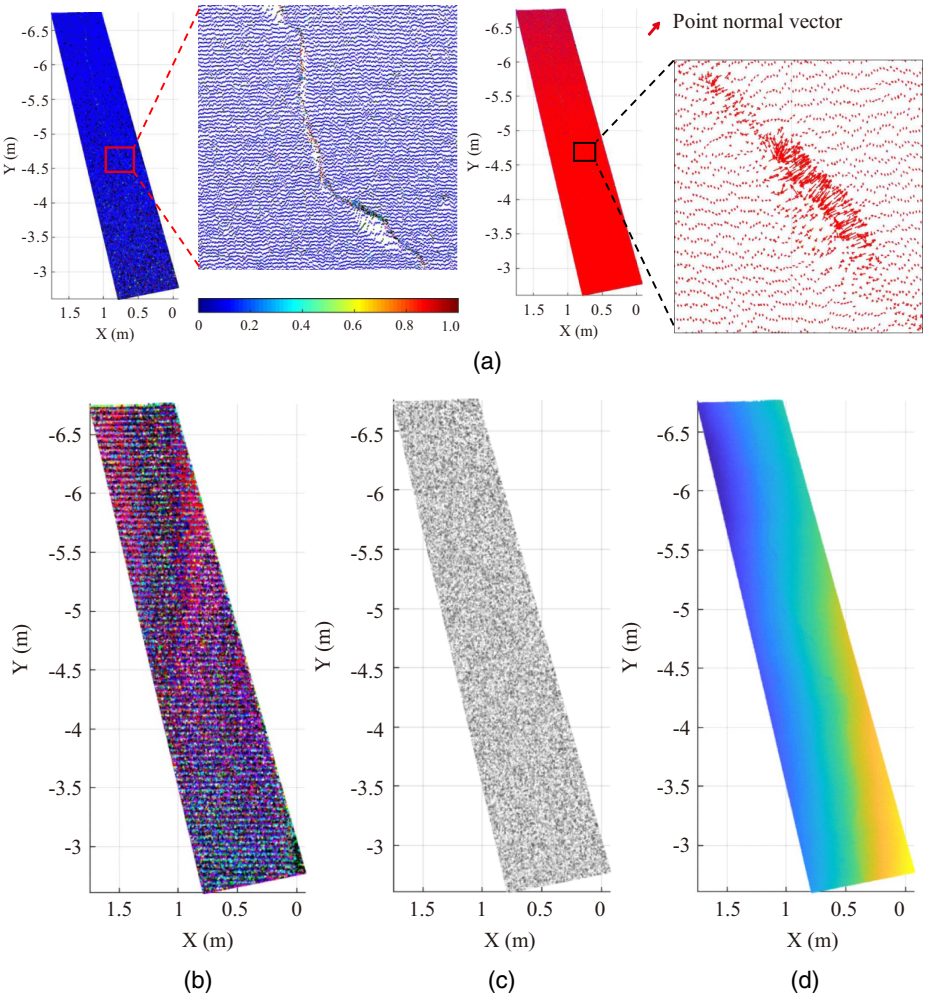

Fig. 3. Point cloud mapped based on different parameters: (a) point normal; (b) point curvature; (c) point intensity; and (d) point depth.

$$Var(n_p) = \frac{\sum_{i=1}^{N+1} (n_i - \bar{n})^2}{N+1} \quad (1)$$

where $\bar{n}$ = average of normal of the given point and its nearest points; n_i = point normal of the ith nearest point of a given point; and N = number of the nearest points which can be determined through the kNN algorithm, as introduced in the previous section.

Because of the roughness of the ground surface, larger point normal variances were observed not only on the cracks, but also on the dents on the concrete plane. The k-means clustering analysis was then performed to separate the whole point cloud into two groups-ground surfaces with lower normal variances and crack and dent regions with higher normal variances, based on the calculation of the point normal variance (Cheung 2003). The k-means algorithm is a popular tool to conduct the data partition based on the distance to the cluster center (Hamerly and Elkan 2004), and the function of k-means is available for this algorithm in MATLAB. Both point normal and normal variance calculations highly depend on the N, and careful attempts are required to select the optimal one. For the surface crack, the point cloud was not spaced with a uniform interval because the scanning distance between the scanner and the object varies with locations, causing differences in the point density which was defined as the number of points per unit volume associated with the query point in a 3D level [Eq. (2)]

$$D_p = \frac{N_p}{V_p} \quad (2)$$

where D_p indicates the point density; and N_p = point number within a 3D space with a volume of V_p. For the convenience of calculation, Eq. (2) was simplified as:

$$D_p = \frac{1}{4/3 \cdot \pi \cdot r^3} \quad (3)$$

where r = radius of the sphere under consideration and can be estimated based on the 4th nearest neighbor distance of the query point. The average point density for the whole point cloud was calculated based on the average [mean($dist_{4th}$)] and standard deviation [std($dist_{4th}$)] of 4th nearest neighbor distances ($dist_{4th}$) of all points in the point cloud [Eq. (4)] (Ester et al. 1996; Riquelme et al. 2014):

$$r = mean(dist_{4th}) + 2 \cdot std(dist_{4th}) \quad (4)$$

Fig. 4(a) illustrates the point density distribution in the ground crack case. The point density gradually decreased from the bottom to the top which had a further scanning distance from the scanner, and the average point density of entire point clouds was 3.3969 points/cm^3. Accordingly, scanning with a shorter distance acquired more points under the same condition, indicating more details on the ground surface were captured. To eliminate the

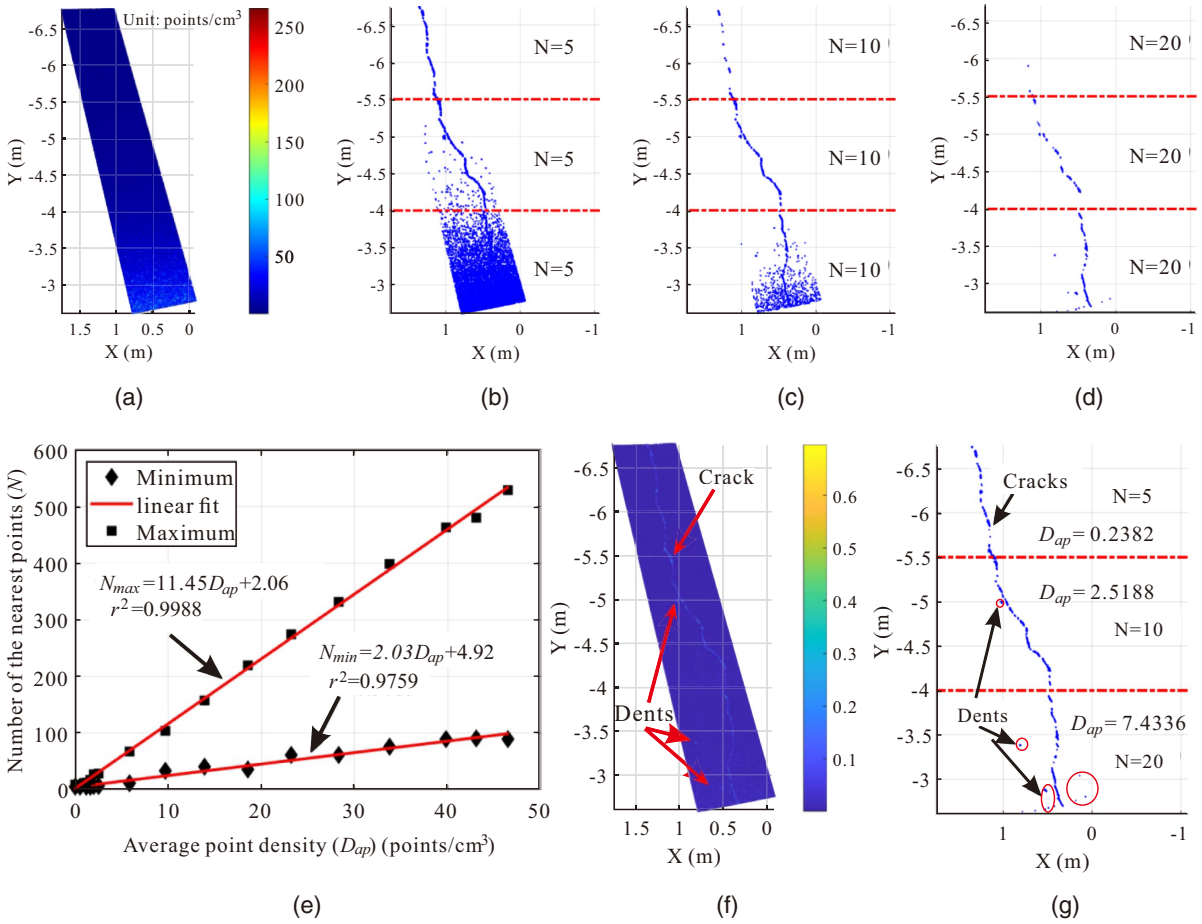

Fig. 4. Cracks and dents extraction from the point cloud: (a) point density distribution; (b) clustering analysis with $N = 5$; (c) clustering analysis with $N = 10$; (d) clustering analysis with $N = 20$; (e) relationship between average point density and number of the nearest points; (f) normal variance calculation with different N; and (g) cracks and dents detection after clustering analysis.

effects of point density differences on crack detection, it is suggested to calculate the point normal and point normal variance based on the point clouds with similar average point densities. In this case, the point cloud started from −6.7648 m and ended at −2.6071 m with a length of 4.1577 m along the Y-axis direction. Theoretically, the more segments the point cloud was equally divided into, the closer the average point density of each segment was, and, however, the more processing time was required accordingly. To maintain a balance between precision and efficiency, the point cloud with a significant difference in point density was suggested to be divided into at least three segments. Therefore, the point cloud of the concrete ground case was discretized into three equal segments along the Y-axis with a similar average point density for each one: 0.2382 points/cm^3 ($Y \le -5.4$ m), 2.5188 points/cm^3 (-5.4 m $< Y < 4.0$ m), and 7.4336 points/cm^3 ($Y \ge -4.0$ m). Figs. 4(b–d) show the cracks and dents detection with the same number of neighbor points for the entire scanning region after clustering analyses: $N = 5$, 10, and 20, respectively. A high N value indicates more points are involved to calculate the point normal, ignoring the local difference between the query point and its neighbor points and vice versa. For the regions with a high point density ($Y \ge -4.0$ m), a smaller N increased the difference in the point normal, leading to too many small-scale dents identified in addition to cracks. On the other hand, the cracks in the regions with a low point density ($Y \le -5.4$ m) could be mistakenly removed from the point cloud when N was specified as a larger value, emphasizing too much the global features of point normal rather than local features. Therefore, the optimal N should be selected according to the point density. Serials of point clouds with different average point densities were generated from segment data of this example (region within -5.4 m $< Y < 4.0$ m in this example) using the pcdownsample function in MATLAB software, and the original average point densities were 2.5188 and 46.4127 points/cm^3, respectively. The corresponding minimum and maximum N were estimated for each point cloud through multiple adjustments until good crack detections were achieved. Linear relationships were observed between the average point density (D_{ap}) and N, as expressed in Eq. (5) [Fig. 4(e)]:

$$N_{\max} = 11.45 \cdot D_{ap} + 2.06$$
$$N_{\min} = 2.03 \cdot D_{ap} + 4.92 \quad (5)$$

According to Eq. (5), the appropriate range of N for each segment was determined based on the average point density of the point cloud. Accordingly, the range of neighbor points numbers for each segment was set as $5 \le N \le 5$ ($Y \le -5.4$ m), $10 \le N \le 31$ (-5.4 m $< Y < 4.0$ m), and $20 \le N \le 87$ ($Y \ge -4.0$ m). Because the computational time increased with the increase of N, the minimum of N was selected to enhance the data processing efficiency. In this manner, reasonable results of point normal variance calculation and cracks and dents detection were achieved through the k-means clustering analysis [Figs. 4(f and g)].

J. Infrastruct. Syst., 2023, 29(2): 04023005

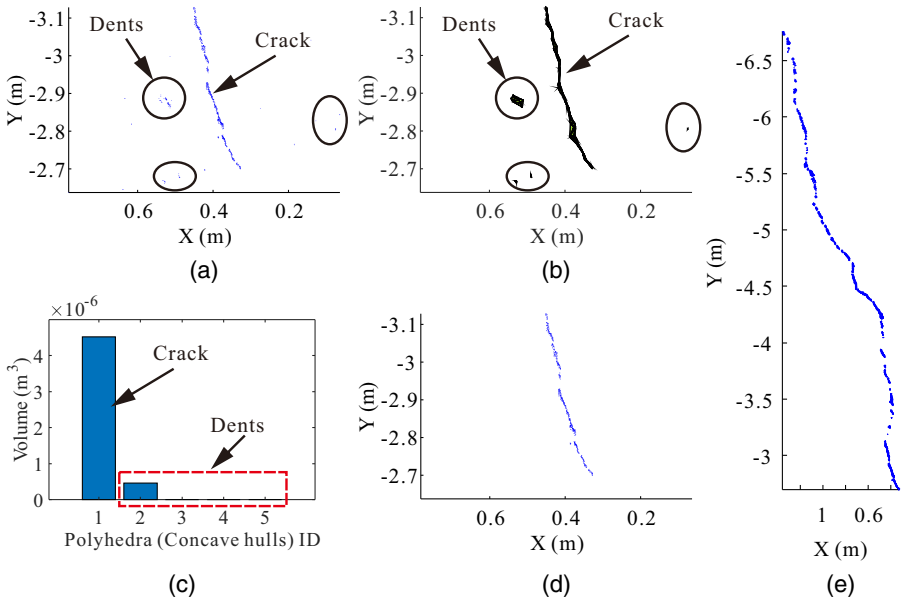

Fig. 5. Dents removal from the point cloud of boundaries: (a) point clouds of crack and dents; (b) 3D reconstruction of crack and dents; (c) volume distribution of dents and crack; (d) point cloud of the portion of the crack; and (e) point cloud of the whole crack.

Small-Scale Dents Removal

The geometric characteristics varied from cracks to dents: dents were small-size and isolated pits on the ground surface, and the cracks were characterized by continuous curves. In addition, dents were distributed on the ground surface one by one with less connectivity, resulting in a smaller volume. Therefore, cracks can be separated from dents based on the differences in their dimensions, such as aspect ratio, area, and volume. In this study, the volume was selected as the judging parameter to remove the points on the small-scale dents. To calculate the volume, 3D models of cracks and dents were reconstructed using the alpha-shape algorithm. The alpha-shape algorithm is an effective tool to define both the convex and nonconvex envelopes of points depending on the alpha value. An alpha value of 1 generates a convex hull (Edelsbrunner et al. 1983). However, due to the concave shape of cracks and dents, a nonzero alpha radius was automatically determined to estimate their concave hulls and compute their volumes using the critical Alpha function in MATLAB. Then, an automated method was proposed to determine the volume threshold for removing the dent points through calculating the maximum value of volume. When the convex hull volume of points was lower than the volume of thresholds, these points were considered dents and were removed from the point clouds.

In this example, the majority of dents were located in the bottom region of the crack. Fig. 5 demonstrates the procedure of dents removal using the detected boundaries in the range from −2.64 to −3.13 along the Y-axis. Fig. 5(a) shows the originally detected point clouds of crack and dents in this region. The polyhedrons with different sizes in Fig. 5(b) were the concave hulls of the crack and dents reconstructed using the alpha-shape algorithm with a 0.004 m alpha radius. More continuous and larger polyhedra were generated for crack points, compared with the dent points. Fig. 5(c) illustrates the volume distributions of the dent and crack polyhedra. Because of the specific geometric characteristics, the volumes of dent polyhedra were much smaller than the volumes of the cracks. Therefore, the polyhedron with the largest volume was treated as the crack, which was automatically determined by calculating the maximum volume. Meanwhile, the dents—the polyhedrons with smaller volumes—were removed from the point cloud of boundaries [Fig. 5(d)]. Fig. 5(e) shows the point cloud of the entire crack after all dents were removed in this example. A good agreement was observed between the crack detection in Fig. 5(d) and the real situation in Fig. 2(a), revealing the alpha-shape algorithm can accurately capture the geometrical features of cracks and dents and distinguish them.

Cracks Characterization

Both the projected and real dimensions of the crack were determined in this study. Results were compared with those from manual measurements during the crack condition survey.

Projected Dimension of Crack

The point cloud of the detected crack was projected into a horizontal plane to measure its projected dimensions. To perform the projection, a new coordinate system is needed to be defined, in which the major axis (longitudinal direction) of a crack is selected as the X-axis, the middle axis is the y-axis, and the minor axis is the z-axis. In Euclidean space, point cloud projection is treated as a rigid transformation that can be implemented based on the rotation matrix $\mathbf{R}$ and translation matrix $\mathbf{T}$ [Eq. (6)]

$$PC^* = PC \cdot \mathbf{R} + \mathbf{T} \tag{6}$$

where PC^* = point clouds of cracks after projection; PC = original point clouds of cracks; $\mathbf{R}$ is represented by an orthogonal matrix which can be determined using the PCA algorithm; and $\mathbf{T}$ is estimated by the difference of minimum on XYZ between original and rotated point clouds. The largest distances of projected point cloud along the major, middle, and minor axis are regarded as the projected length, width, and depth of the crack, respectively.

Fig. 6(a) illustrates the results of coordinate projection of the crack on the concrete ground. The black lines indicate the principal axes of the crack and the line length is its projected dimension. As summarized in Table 2, the projected dimension of this crack was 4.185 m in length, 0.338 m in width, and 0.013 m in depth.

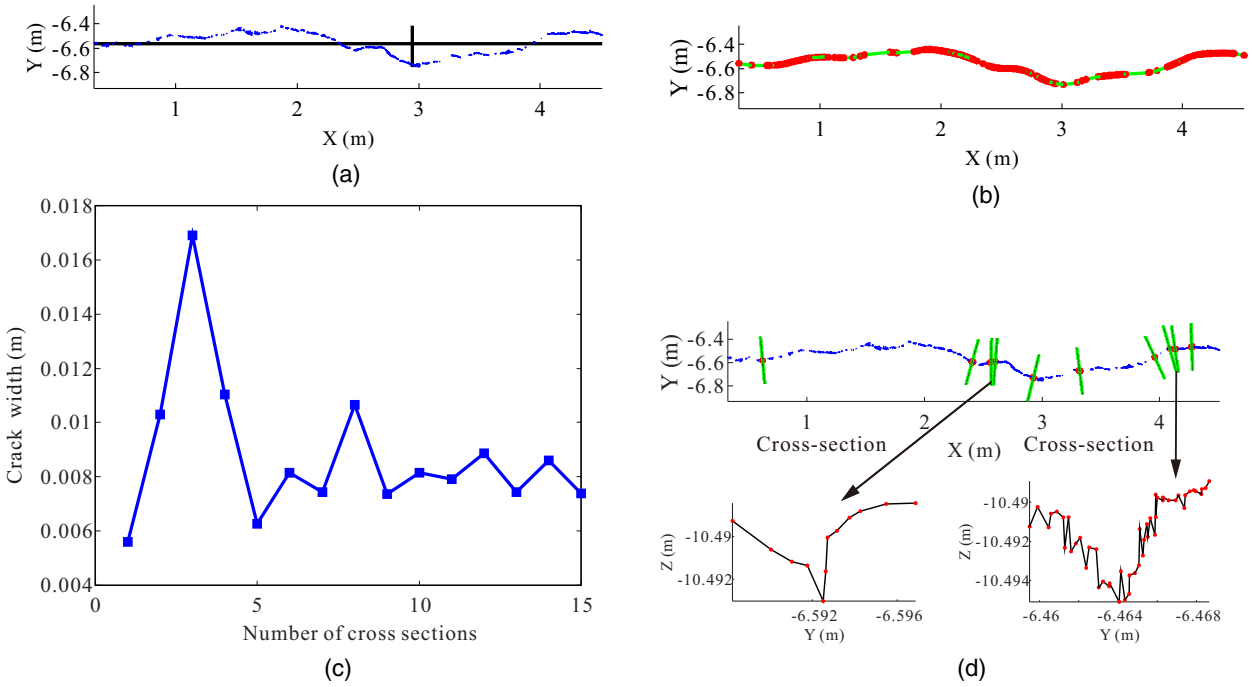

Fig. 6. Crack characterization using projection and curve-skeleton methods: (a) the projection of a crack on horizontal plane; (b) the skeleton of a crack; (c) average width changes with the number of cross sections randomly selected from the crack point cloud; and (d) the locations of 10 cross sections.

Table 2. Summary of dimensions of cracks

			Manual measurement			Projection algorithm			Curve-skeleton algorithm		
Cases	Location	Point amount	Length (m)	Width (m)	Depth (m)	Length (m)	Width (m)	Depth (m)	Length (m)	Width (m)	Depth (m)
Ground surface	—	4,183	4.18	0.009	—	4.185	0.338	0.013	4.285	0.008	0.003
Stair	Upper	3,917	0.275	0.015	0.013	0.268	0.07	0.05	0.339	0.018	0.012
	Middle	4,096	0.273	0.012	0.012	0.272	0.039	0.03	0.298	0.011	0.017
	Lower	18,778	0.369	0.014	0.025	0.357	0.085	0.038	0.440	0.021	0.012

The projected dimension represents the minimum external cuboid containing the cracks on the concrete structures.

Real Dimension of Crack

Due to the fact that the crack is often a curve rather than a straight line, the curve-skeleton of the point cloud was adopted to calculate the real length of cracks. Curve-skeleton is a simplified version of a 3D object with 0 volume, which provides a compact and intuitive representation of complex geometries and can capture their essential geometric features (Cornea et al. 2007; Au et al. 2008). Extraction of the curve-skeleton is useful for reducing the data dimension in many applications, such as path planning, shape registration and retrieval, and plant morphological traits (Falcão et al. 2017). In this study, the L_1-median skeleton algorithm was used to extract the curve-skeletons of cracks (Huang et al. 2013), and the open-source code of this algorithm is available on the website (https://vcc.tech/research/2013/L1skeleton). L_1-median, also known as the geometric median, is the point with a minimum sum of the Euclidean distance to all surrounding points. L_1-median can be approximately calculated using an iterative procedure (Bose et al. 2003). Fig. 6(b) demonstrates the curve-skeletons (lines) extraction of cracks from the point cloud, and the accumulation distance among the key points (dots) was determined to represent the actual length of cracks. The actual length of this crack is 4.285 m as shown in Table 2.

The cracks on concrete structures are often characterized by irregular shapes, causing great data dispersion only through a single measurement. The dimension of the crack varied from location to location, and it was very difficult to obtain the accurate dimensions of the crack only through one single cross section. Therefore, multiple measurements were required to enhance the measuring accuracy. Through trial and error, it was found that the crack width tended to be stable when more than 10 cross sections were chosen [Fig. 6(c)]. Therefore, in this study, 10 cross sections were randomly selected to eliminate the measurement error due to the data dispersion. Fig. 6(d) shows that locations of 10 cross sections were automatically and randomly chosen along the crack to determine its real width and depth, each of which was perpendicular to the crack. These sections can be defined by the points with a distance to the plane on either side less than the tolerance. Theoretically, the points with zero distances to the cross section will be regarded to be on this cross section. However, it is impossible to extract these points by specifying the tolerance as zero, because of the noncontinuity of the point clouds. The tolerance selection highly depends on the resolution and point density of the point clouds of cracks. The higher the resolution and point density, the smaller the tolerance

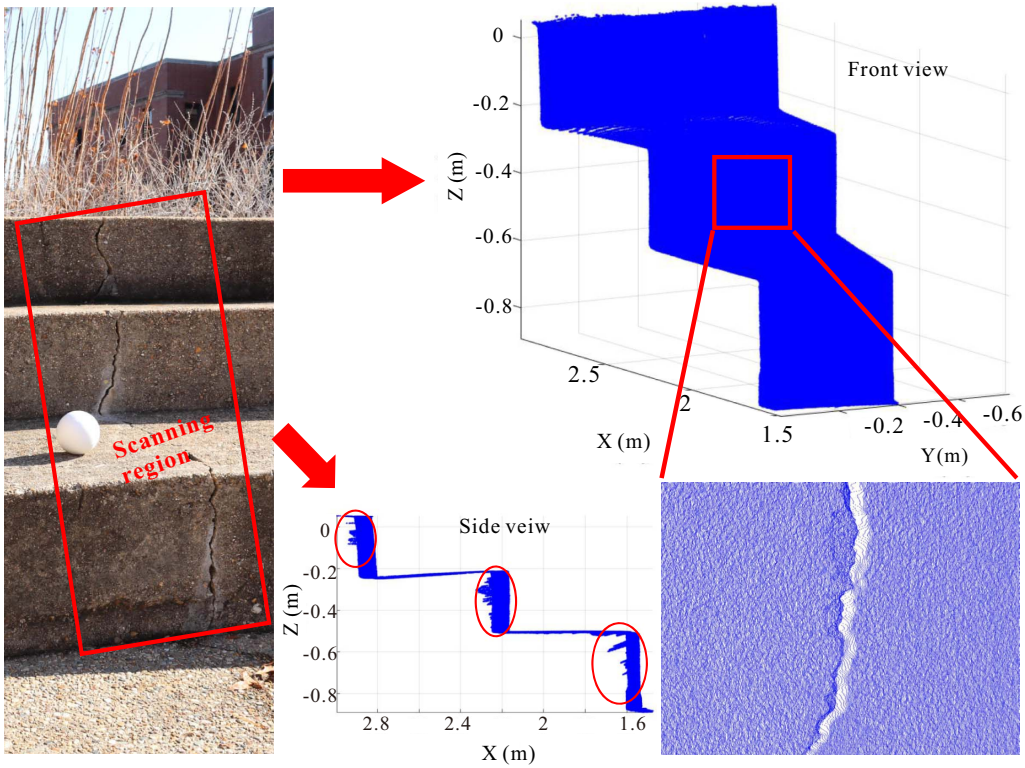

Fig. 7. Point clouds collection of cracks in the stair case.

(Maalek and Lichti 2021). After many attempts, the tolerance was set as 1 mm in this study. Two cross sections were selected to demonstrate the typical geometry features in the Y–Z plane and were roughly v-shaped as shown in Fig. 6(c). The maximum distances along the width (Y-axis) and depth (Z-axis) direction at each section were determined, and the average of 10 sections was considered as the real width and depth of the crack. The circles are the randomly selected cross sections, and the points located on the circles can be extracted based on the distance tolerance (points). The crack has an actual width of 0.008 m and an actual depth of 0.003 m as summarized in Table 2.

Manual Crack Measurement

A cracking condition survey was also conducted to manually measure the length and width of the crack according to the Distress Identification Manual for the Long-Term Pavement Performance Program (Miller and Bellinger 2014), and its length and width are also included in Table 2.

The distance between the two ends of the crack was measured along the X direction to represent the length of this crack using a projection algorithm. Thus, the length of this crack obtained by manual measurement was less than those for the curve-skeleton algorithm, where the length of the curved crack was measured. Additionally, there are different definitions of width and depth in the three methods. The maximum distances among the points along YZ directions were regarded as width and depth in the projection method, whereas the perpendicular distance between two lines of the crack was the width in the manual and real dimension measurements. Due to the curve-shape of the crack, the projected width and depth of this crack were larger than those obtained by the manual measurement and cross-section method. As seen from Table 2, the lengths obtained from the manual measurement and projection algorithm were close (4.18, and 4.185 m, respectively), but smaller than those obtained from the curve-skeleton algorithm (4.285 m). The results were reasonable because measurements obtained from the 3D reconstruction can obtain more accurate results with more detailed information regarding the cracking. In addition, similar results confirmed a good agreement between the new method and the current commonly used manual measurement method.

Case Study

To test the robustness of the proposed method under more complex situations, cracks on a stair with multiple planes were selected as a case study, and the same laser scanner was used to collect the point cloud of the stair, oriented approximately perpendicular to the three vertical surfaces (Fig. 7). The scan parameters are summarized in Table 1. The shapes and dimensions of cracks varied from stair to stair: the crack on the lower stair had the maximum average length and depth (0.369 and 0.025 m, respectively), whereas the crack on the upper stair had the maximum average width (0.015 m). The whole scanning lasted less than 10 min, and the resolution of the obtained point cloud was approximate 3 mm, which made it possible to capture more details and the points inside the cracks. After removing the undesired and noise data in preprocessing, there were 1,496,291 points remaining. A similar point density was observed in these stair planes, and optimal N selection did not consider the effect from the point density in this case. The front and side views of the stair are also shown in Fig. 7, and the point distribution in crack areas is different from that in noncrack areas. Sparser points were observed in the crack area (front view). Because points inside of the crack were collected during laser scanning, more irregularity was found in the crack areas compared with noncrack areas (side view).

Figs. 8(a–n) show the changes of point normal with a different number of nearest neighbor points in the stair case. When N was set

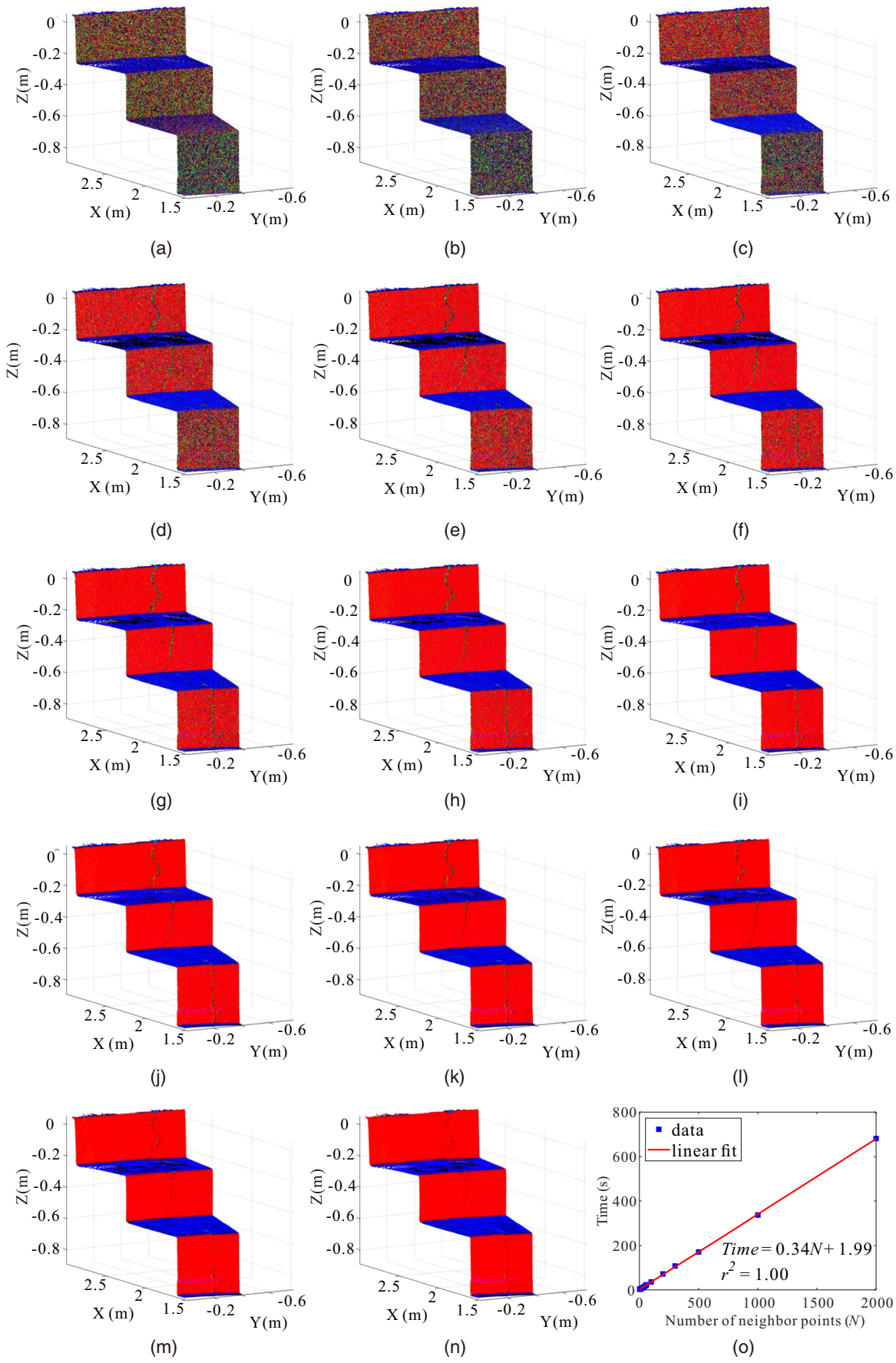

Fig. 8. Variance of point normal vectors and computational time of point normal calculations with different neighboring points: (a) $N = 3$; (b) $N = 5$; (c) $N = 10$; (d) $N = 20$; (e) $N = 30$; (f) $N = 40$; (g) $N = 50$; (h) $N = 60$; (i) $N = 100$; (j) $N = 200$; (k) $N = 300$; (l) $N = 500$; (m) $N = 1{,}000$; (n) $N = 2{,}000$; and (o) plot of computational time versus N.

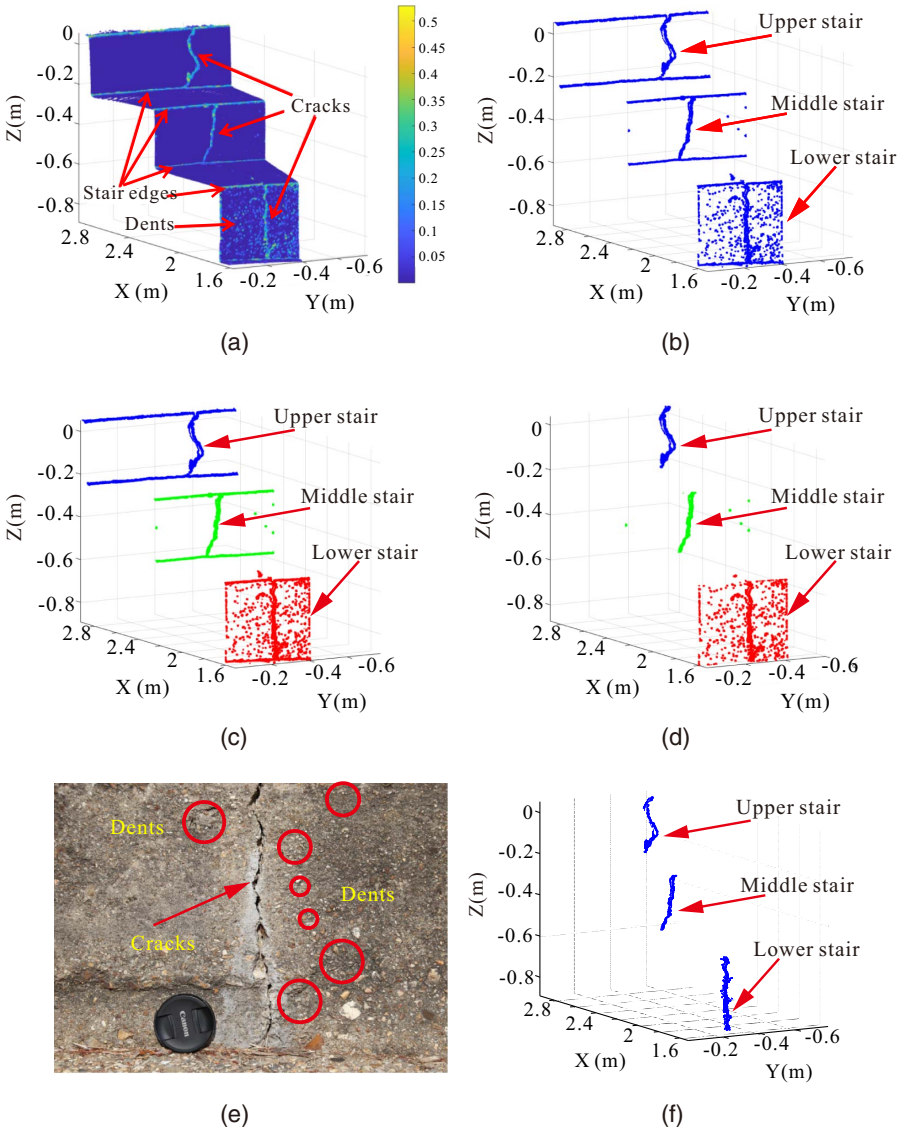

Fig. 9. Cracks detection from point clouds in the stair case: (a) normal variance distribution; (b) cracks, stair edges, and dents extraction; (c) second clustering; (d) horizontal stair edges removal; (e) photo of the lower stair surface; and (f) small-scale dents removal.

to less than 100, more differences in the point normal distribution were observed, even on the relatively smooth stair planes. When N was specified as more than 500, the point normal distribution cannot accurately reflect the cracks' positions. Good results were obtained when choosing the N ranging from 100–500 points, matching the N range (100 points $\leq N \leq$ 539 points) calculated based on the average point density (46.8768 points/cm^3) using Eq. (5). Furthermore, the exact computational time for point normal calculations with different N was measured using Tic & Toc functions in MATLAB software. Fig. 8(o) illustrates the curve of elapsed time versus N considered in the point normal calculation, and a linear relationship between them was observed. The computational time increased with the increase of N. To save the computational time and improve computational efficiency, 100 neighbor points were eventually selected to calculate the point normal and point normal variance in this example.

Fig. 9(a) shows the normal variance distribution of the stair point cloud based on Eq. (1) with considering 100 nearest neighbor points. It is obvious that the cracks, stair edges, and dents had high normal variance compared with horizontal and vertical stair planes. They were identified from point clouds using the k-means clustering algorithm [Fig. 9(b)]. The horizontal stair edges and vertical cracks were detected in the upper stair region. Many dents on the lower two stair surfaces were also identified, besides the edges and cracks.

Note that the situation of the ground case is simpler than this stair case, because cracks only need to be identified from one single ground surface without interference from multiple planes. It is also needed to remove the edges from the point clouds in the stair case in addition to the dents. The stair edges are located on the intersections of two adjacent stair planes and aligned horizontally; as a result, the points on the stair edges have similar z-coordinates. Consequently, they can be removed by specifying the lower and upper margins. Another k-means clustering was performed to classify all boundary points (cracks, dents, and stair edges) into three sets based on the stair location (x-coordinates) because there were three stairs in total in this case. The second clustering results are shown in Fig. 9(c), and detected points in the upper, middle, and

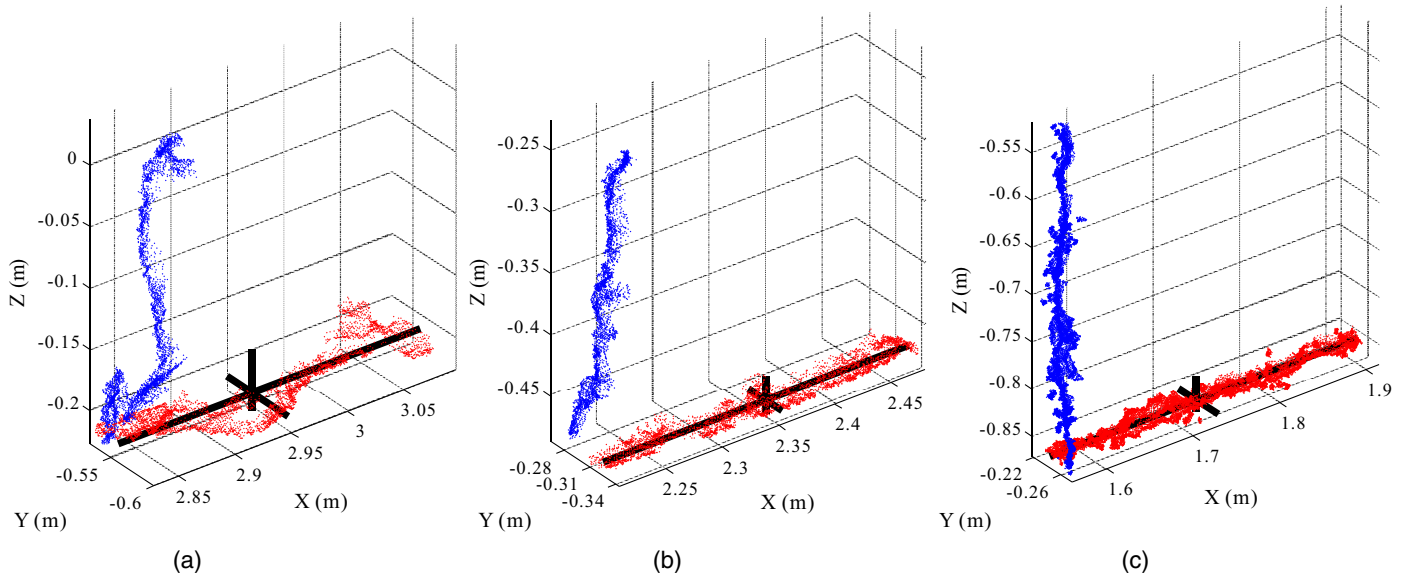

Fig. 10. Projection of the crack point clouds: (a) upper stair; (b) middle stair; and (c) lower stair (original point clouds are vertical point clouds after transformation are horizontal, and principal axes of point clouds are represented by thick straight line).

lower stairs were separated by their x-coordinates, respectively. If the points' z-coordinates were less than the lower margin but larger than the upper margin, they were considered as the points located on the horizontal stair edges, and then removed after the second clustering. For example, in the case of the upper stair, the maximum and minimum z-coordinates of all points' z-coordinates were 0.053 and −0.2486 m. The upper and lower margins were set as 0.015 and 0.020 m, respectively, and the points with z-coordinates ranging from −0.2286 to 0.038 m were retained as the point clouds of cracks and dents. It is suggested that the margins be selected based on the thickness of points on the stair edges. Fig. 9(d) shows the point clouds of cracks and dents after removing the horizontal edges in the upper, middle, and lower stairs, respectively.

Fig. 9(e) shows the real condition of the lower stair. Its surface was not a perfect plane with many dents on it, which was consistent with the analysis results. Due to the high resolution of TLS, these tiny damages on the concrete surfaces could be captured and were removed through the alpha-shape algorithm and volume threshold. Fig. 9(f) shows the final results of crack detection from the point clouds.

Subsequently, the procedure of crack characterization was performed to determine the projected and real dimension of cracks in the stair. Fig. 10 shows the projection results obtained using the PCA algorithm, and the original point clouds of three cracks are vertical and projected are horizontal. In the projected point clouds, the orthogonal straight lines indicate the major, middle, and minor axes, respectively. Fig. 11 shows the curve-skeletons of cracks in the stair which were found using the L_1-median skeleton algorithm and used to measure the real length of cracks. The lines are the curve-skeletons, and balls are the key points. Ten cross sections perpendicular to the crack were selected at random for each crack to calculate the real width and depth of the cracks. Additionally, v-shaped cracks were observed on the cross section (Fig. 12). The results are summarized in Table 2. Similar to the ground case,

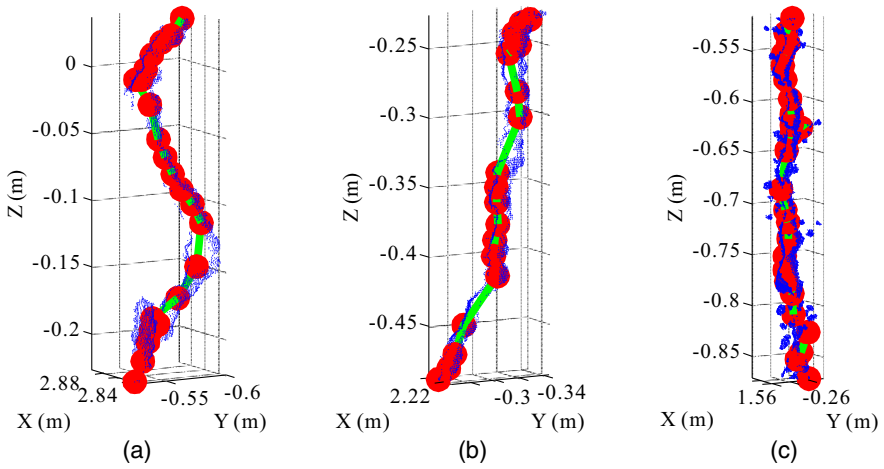

Fig. 11. Curve-skeleton of the crack point clouds: (a) upper stair; (b) middle stair; and (c) lower stair (green lines are the curve skeletons, red balls are the key points in skeletons, and blue dots are the point clouds of cracks).

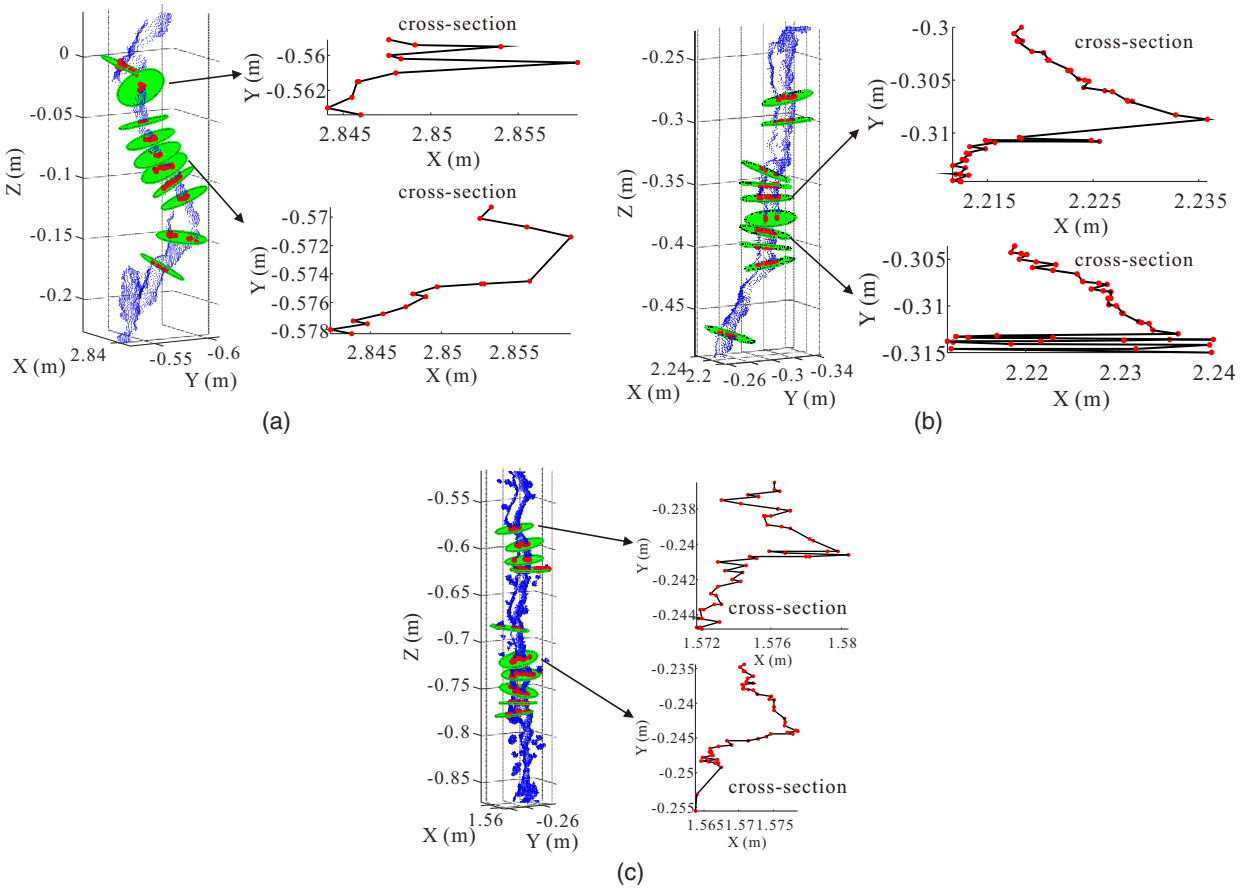

Fig. 12. Ten cross sections selected in the point clouds of cracks: (a) upper stair; (b) middle stair; and (c) lower stair (circles are the cross sections, and dots are the points on the cross sections).

Table 3. Computational time of crack detection and characterization for two cases

Case	Computational time for point normal calculation and cracks-dents extraction (s)	Computational time for small-scale dents removal and dimension measurement (s)	Total computational time (s)	Computer configuration
Ground surface	16.661	24.682	41.343	Laptop brand: Dell Precision 5530 BTX BASE Processor: Intel (R) Core (TM) i9-= 8950HK Six Core, CPU @ 2.90 GHz 2.90 GHz Installed memory (RAM): 16.00 GB (15.7 GB usable) Operating system: Windows 10 Home Edition (64-bit)
Stair	85.305	12.749	98.054	

the real dimensions matched the manual measurements, but with higher accuracy, indicating the good performance of the proposed methods. The developed method can automatically capture more details of the cracking from 3D point clouds. It is used to conduct complete processing and analysis for different conditions (cracks on a ground surface and cracks on a stair with multiple planes) with accurate results.

The computational time for each procedure in two cases was recorded under the same computer configuration, using the Tic & Toc functions in MATLAB software. Table 3 shows the duration that the developed method was taken for each step during the crack detection and characterization. The total computational time included three parts: (1) point normal calculation and crack and dents based on point normal variance, (2) small-scale dents removal, projection dimension of crack, and real dimension of crack (width and depth), and (3) real dimension of crack (length). Eventually, 41.343 s was cost totally for the concrete ground case and 98.054 s for the concrete stair case, respectively, indicating the high efficiency and feasibility of the proposed method in this study.

Conclusions

An approach was developed to automatically detect and characterize the cracks on concrete structures from the 3D point clouds in this study. The point normal variance was selected as the index to locate the cracks, and two methods (coordinate transformation and curve-skeletons and cross sections) were used to determine the

J. Infrastruct. Syst., 2023, 29(2): 04023005

projected and real dimensions of cracks, respectively. In the crack detection process, kNN and PCA algorithms were used to determine the point normal, and k-means clustering, and alpha-shape algorithms were employed to remove the undesired data concerning surfaces, horizontal stair edges, and small dents. In the crack characterization process, the coordinate transformation was performed to find the major, middle, and minor axes of cracks to calculate the projected dimensions. Furthermore, curve-skeletons and cross sections of cracks were extracted to represent the real dimensions. The example and one case study demonstrated good agreements of results between the manual measurements and the real dimensions of cracks which were calculated using the developed method. In summary, the developed method enables a fast, accurate measurement and more comprehensive analysis for crack detection and characterization.

It was found that the point normal calculation highly depends on the number of neighbor points. The number of nearest neighbor points was suggested to be selected taking the point density into account. It is recommended that more case studies in various infrastructures such as bridges and buildings are needed to further validate the approach developed.

This method was developed to identify and characterize cracks only based on the point clouds. Therefore, the method can be suitable for any other measuring techniques which collect the high-resolution point clouds of the cracks, such as portable laser scanning and photogrammetry. More case studies using other measuring techniques are needed to explore the wider application of this method. For the small-scale cracks (e.g., less than a few millimeters in width), the terrestrial laser scanner is not able to collect detailed morphological information inside the cracks due to its resolution limitations. In this case, additional information such as color is highly recommended to be included to identify the cracks instead of the geometric data only. This study only focused on the automated detection and characterization of the individual crack, and the multiple cracks that overlapped with each other were not involved. The point normal variance can still be extended to detect multiple cracks in future work.

Data Availability Statement

All data used during the study are available upon request.

Acknowledgments

This work was supported by the National Key R&D Program of China (No. 2017YFC1501303). The first author of this paper is grateful to the Chinese Scholarship Council for providing an opportunity to conduct the research described in this paper as a visiting research scholar at the Missouri University of Science and Technology in Rolla, Missouri. Mr. Ruiyang Zhang is acknowledged for his help in data collection.

References

Au, O. K. C., C. L. Tai, H. K. Chu, D. Cohen-Or, and T. Y. Lee. 2008. "Skeleton extraction by mesh contraction." *ACM Trans. Graphics* 27 (3): 1–10. https://doi.org/10.1145/1360612.1360643.

Avila, M., S. Begot, F. Duculty, and T. S. Nguyen. 2014. "2D image based road pavement crack detection by calculating minimal paths and dynamic programming." In *Proc., 2014 IEEE Int. Conf. on Image Processing (ICIP)*, 783–787. New York: IEEE.

Bandis, S. C., A. C. Lumsden, and N. R. Barton. 1983. "Fundamentals of rock joint deformation." *Int. J. Rock Mech. Min. Sci. Geomech. Abstr.* 20 (6): 249–268. https://doi.org/10.1016/0148-9062(83)90595-8.

Bose, P., A. Maheshwari, and P. Morin. 2003. "Fast approximations for sums of distances, clustering and the Fermat–Weber problem." *Comput. Geom.* 24 (3): 135–146. https://doi.org/10.1016/S0925-7721(02)00102-5.

Cha, Y. J., W. Choi, and O. Büyüköztürk. 2017. "Deep learning-based crack damage detection using convolutional neural networks." *Comput.-Aided Civ. Infrastruct. Eng.* 32 (5): 361–378. https://doi.org/10.1111/mice.12263.

Cheung, Y. M. 2003. "k*-Means: A new generalized k-means clustering algorithm." *Pattern Recognit. Lett.* 24 (15): 2883–2893. https://doi.org/10.1016/S0167-8655(03)00146-6.

Cornea, N. D., D. Silver, and P. Min. 2007. "Curve-skeleton properties, applications, and algorithms." *IEEE Trans. Visual. Comput. Graphics* 13 (3): 530–548. https://doi.org/10.1109/TVCG.2007.1002.

Deng, Z., X. Zhu, D. Cheng, M. Zong, and S. Zhang. 2016. "Efficient kNN classification algorithm for big data." *Neurocomputing* 195 (Jun): 143–148. https://doi.org/10.1016/j.neucom.2015.08.112.

Dung, C. V. 2019. "Autonomous concrete crack detection using deep fully convolutional neural network." *Autom. Constr.* 99 (Mar): 52–58. https://doi.org/10.1016/j.autcon.2018.11.028.

Edelsbrunner, H., D. G. Kirkpatrick, and R. Seidel. 1983. "On the shape of a set of points in the plane." *IEEE Trans. Inf. Theory* 29 (4): 551–559. https://doi.org/10.1109/TIT.1983.1056714.

Ester, M., H. P. Kriegel, J. Sander, and X. Xu. 1996. "A density-based algorithm for discovering clusters in large spatial databases with noise." In *Proc., KDD*, 226–231. Portland, OR: Association for the Advancement of Artificial Intelligence.

Falcão, A., C. Feng, J. Kustra, and A. Telea. 2017. "Multiscale 2D medial axes and 3D surface skeletons by the image foresting transform." In *Skeletonization: Theory, methods and applications*, 43–70. Cambridge, UK: Academic Press.

Fei, Y., K. C. Wang, A. Zhang, C. Chen, J. Q. Li, Y. Liu, and B. Li. 2019. "Pixel-level cracking detection on 3D asphalt pavement images through deep-learning-based cracknet-V." *IEEE Trans. Intell. Transp. Syst.* 21 (1): 273–284. https://doi.org/10.1109/TITS.2019.2891167.

Ge, Y., H. Tang, D. Xia, L. Wang, B. Zhao, J. W. Teaway, and T. Zhou. 2018. "Automated measurements of discontinuity geometric properties from a 3D-point cloud based on a modified region growing algorithm." *Eng. Geol.* 242 (Aug): 44–54. https://doi.org/10.1016/j.enggeo.2018.05.007.

Gui, R., X. Xu, D. Zhang, H. Lin, F. Pu, L. He, and M. Cao. 2018. "A component decomposition model for 3D laser scanning pavement data based on high-pass filtering and sparse analysis." *Sensors* 18 (7): 2294. https://doi.org/10.3390/s18072294.

Hamerly, G., and C. Elkan. 2004. "Learning the k in k-means." In Vol. 16 of *Advances in neural information processing systems*, 281–288. San Mateo, CA: Morgan Kaufmann Publishers.

Hoang, N. D., Q. L. Nguyen, and D. Tien Bui. 2018. "Image processing–based classification of asphalt pavement cracks using support vector machine optimized by artificial bee colony." *J. Comput. Civ. Eng.* 32 (5): 04018037. https://doi.org/10.1061/(ASCE)CP.1943-5487.0000781.

Huang, H., S. Wu, D. Cohen-Or, M. Gong, H. Zhang, G. Li, and B. Chen. 2013. "L_1-medial skeleton of point cloud." *ACM Trans. Graphics* 32 (4): 65. https://doi.org/10.1145/2461912.2461913.

Huang, H. W., Q. T. Li, and D. M. Zhang. 2018. "Deep learning based image recognition for crack and leakage defects of metro shield tunnel." *Tunnelling Underground Space Technol.* 77 (Jul): 166–176. https://doi.org/10.1016/j.tust.2018.04.002.

Jahanshahi, M. R., F. Jazizadeh, S. F. Masri, and B. Becerik-Gerber. 2013. "Unsupervised approach for autonomous pavement-defect detection and quantification using an inexpensive depth sensor." *J. Comput. Civ. Eng.* 27 (6): 743–754. https://doi.org/10.1061/(ASCE)CP.1943-5487.0000245.

Jiang, R., D. V. Jáuregui, and K. R. White. 2008. "Close-range photogrammetry applications in bridge measurement: Literature review."

Measurement 41 (8): 823–834. https://doi.org/10.1016/j.measurement.2007.12.005.

Jovančević, I., H. H. Pham, J. J. Orteu, R. Gilblas, J. Harvent, X. Maurice, and L. Brèthes. 2017. "3D point cloud analysis for detection and characterization of defects on airplane exterior surface." *J. Nondestr. Eval.* 36 (4): 74. https://doi.org/10.1007/s10921-017-0453-1.

Kaseko, M. S., and S. G. Ritchie. 1993. "A neural network-based methodology for pavement crack detection and classification." *Transp. Res. Part C: Emerging Technol.* 1 (4): 275–291. https://doi.org/10.1016/0968-090X(93)90002-W.

Kim, M. K., H. Sohn, and C. C. Chang. 2014. "Localization and quantification of concrete spalling defects using terrestrial laser scanning." *J. Comput. Civ. Eng.* 29 (6): 04014086. https://doi.org/10.1061/(ASCE)CP.1943-5487.0000415.

Kirschke, K. R., and S. A. Velinsky. 1992. "Histogram-based approach for automated pavement-crack sensing." *J. Transp. Eng.* 118 (5): 700–710. https://doi.org/10.1061/(ASCE)0733-947X(1992)118:5(700).

Klasing, K., D. Althoff, D. Wollherr, and M. Buss. 2009. "Comparison of surface normal estimation methods for range sensing applications." In *Proc., 2009 IEEE Int. Conf. on Robotics and Automation*, 3206–3211. New York: IEEE.

Laefer, D. F., L. Truong-Hong, H. Carr, and M. Singh. 2014. "Crack detection limits in unit based masonry with terrestrial laser scanning." *NDT&E Int.* 62 (Mar): 66–76. https://doi.org/10.1016/j.ndteint.2013.11.001.

Laflamme, S., M. Kollosche, J. J. Connor, and G. Kofod. 2012. "Soft capacitive sensor for structural health monitoring of large-scale systems." *Struct. Control Health Monit.* 19 (1): 70–81. https://doi.org/10.1002/stc.426.

Lee, B. J., and H. D. Lee. 2004. "Position-invariant neural network for digital pavement crack analysis." *Comput.-Aided Civ. Infrastruct. Eng.* 19 (2): 105–118. https://doi.org/10.1111/j.1467-8667.2004.00341.x.

Li, G., X. Zhao, K. Du, F. Ru, and Y. Zhang. 2017. "Recognition and evaluation of bridge cracks with modified active contour model and greedy search-based support vector machine." *Autom. Constr.* 78 (Jun): 51–61. https://doi.org/10.1016/j.autcon.2017.01.019.

Maalek, R., and D. D. Lichti. 2021. "Robust detection of non-overlapping ellipses from points with applications to circular target extraction in images and cylinder detection in point clouds." *ISPRS J. Photogramm. Remote Sens.* 176 (Jun): 83–108. https://doi.org/10.1016/j.isprsjprs.2021.04.010.

Miller, J. S., and W. Y. Bellinger. 2014. *Distress identification manual for the long-term pavement performance program (Fifth revised edition)*. Rep. No. FHWA-HRT-13-092. McLean, VA: Office of Infrastructure Research and Development, Federal Highway Administration.

Mohan, A., and S. Poobal. 2018. "Crack detection using image processing: A critical review and analysis." *Alexandria Eng. J.* 57 (2): 787–798. https://doi.org/10.1016/j.aej.2017.01.020.

Nakaniwa, K., N. Yabuki, D. Nishi, K. Mitani, and M. Matsumoto. 2014. "Development and applications of a total station with a built-in crack scale." In *Proc., 2014 Int. Conf. on Computing in Civil and Building Engineering*, 1755–1762. Reston, VA: ASCE.

Napolitano, R., and B. Glisic. 2019. "Methodology for diagnosing crack patterns in masonry structures using photogrammetry and distinct element modeling." *Eng. Struct.* 181 (Feb): 519–528. https://doi.org/10.1016/j.engstruct.2018.12.036.

Nguyen, T. S., M. Avila, and S. Begot. 2009. "Automatic detection and classification of defect on road pavement using anisotropy measure." In *Proc., 2009 17th European Signal Processing Conf.*, 617–621. New York: IEEE.

Nishiyama, S., N. Minakata, T. Kikuchi, and T. Yano. 2015. "Improved digital photogrammetry technique for crack monitoring." *Adv. Eng. Inf.* 29 (4): 851–858. https://doi.org/10.1016/j.aei.2015.05.005.

Oliveira, H., and P. L. Correia. 2009. "Automatic road crack segmentation using entropy and image dynamic thresholding." In *Proc., 2009 17th European Signal Processing Conf.*, 622–626. New York: IEEE.

Olsen, M. J., F. Kuester, B. J. Chang, and T. C. Hutchinson. 2010. "Terrestrial laser scanning-based structural damage assessment." *J. Comput. Civ. Eng.* 24 (3): 264–272. https://doi.org/10.1061/(ASCE)CP.1943-5487.0000028.

Rabah, M., A. Elhattab, and A. Fayad. 2013. "Automatic concrete cracks detection and mapping of terrestrial laser scan data." *NRIAG J. Astron. Geophys.* 2 (2): 250–255. https://doi.org/10.1016/j.nrjag.2013.12.002.

Riquelme, A. J., A. Abellán, R. Tomás, and M. Jaboyedoff. 2014. "A new approach for semi-automatic rock mass joints recognition from 3D point clouds." *Comput. Geosci.* 68 (Jul): 38–52. https://doi.org/10.1016/j.cageo.2014.03.014.

Ritdumrongkul, S., and Y. Fujino. 2007. "Identification of the location and size of cracks in beams by a piezoceramic actuator–sensor." *Struct. Control Health Monit.* 14 (6): 931–943. https://doi.org/10.1002/stc.204.

Sollazzo, G., K. C. P. Wang, G. Bosurgi, and J. Q. Li. 2016. "Hybrid procedure for automated detection of cracking with 3D pavement data." *J. Comput. Civ. Eng.* 30 (6): 04016032. https://doi.org/10.1061/(ASCE)CP.1943-5487.0000597.

Valença, J., D. Dias-da-Costa, E. N. B. S. Júlio, H. Araújo, and H. Costa. 2013. "Automatic crack monitoring using photogrammetry and image processing." *Measurement* 46 (1): 433–441. https://doi.org/10.1016/j.measurement.2012.07.019.

Valença, J., I. Puente, E. Júlio, H. González-Jorge, and P. Arias-Sánchez. 2017. "Assessment of cracks on concrete bridges using image processing supported by laser scanning survey." *Constr. Build. Mater.* 146 (Aug): 668–678. https://doi.org/10.1016/j.conbuildmat.2017.04.096.

Wang, K. C. 2004. "Challenges and feasibility for comprehensive automated survey of pavement conditions." In *Proc., 8th Int. Conf. on Applications of Advanced Technologies in Transportation Engineering (AATTE)*, 531–536. Reston, VA: ASCE.

Yang, X., H. Li, Y. Yu, X. Luo, T. Huang, and X. Yang. 2018. "Automatic pixel-level crack detection and measurement using fully convolutional network." *Comput.-Aided Civ. Infrastruct. Eng.* 33 (12): 1090–1109. https://doi.org/10.1111/mice.12412.

Zalama, E., J. Gómez-García-Bermejo, R. Medina, and J. Llamas. 2014. "Road crack detection using visual features extracted by Gabor filters." *Comput.-Aided Civ. Infrastruct. Eng.* 29 (5): 342–358. https://doi.org/10.1111/mice.12042.

Zhang, A., K. C. Wang, and C. Ai. 2017a. "3D shadow modeling for detection of descended patterns on 3D pavement surface." *J. Comput. Civ. Eng.* 31 (4): 04017019. https://doi.org/10.1061/(ASCE)CP.1943-5487.0000661.

Zhang, A., K. C. Wang, Y. Fei, Y. Liu, C. Chen, G. Yang, and S. Qiu. 2019. "Automated pixel-level pavement crack detection on 3D asphalt surfaces with a recurrent neural network." *Comput.-Aided Civ. Infrastruct. Eng.* 34 (3): 213–229. https://doi.org/10.1111/mice.12409.

Zhang, A., K. C. Wang, B. Li, E. Yang, X. Dai, Y. Peng, and C. Chen. 2017b. "Automated pixel-level pavement crack detection on 3D asphalt surfaces using a deep-learning network." *Comput.-Aided Civ. Infrastruct. Eng.* 32 (10): 805–819. https://doi.org/10.1111/mice.12297.

Zhang, L., F. Yang, Y. D. Zhang, and Y. J. Zhu. 2016. "Road crack detection using deep convolutional neural network." In *Proc., 2016 IEEE Int. Conf. on Image Processing (ICIP)*, 3708–3712. New York: IEEE.

Zou, Q., Y. Cao, Q. Q. Li, Q. Z. Mao, and S. Wang. 2012. "CrackTree: Automatic crack detection from pavement images." *Pattern Recognit. Lett.* 33 (3): 227–238. https://doi.org/10.1016/j.patrec.2011.11.004.